JOURNAL OF PROPULSION AND POWER
Vol. 11, No. 2, March–April 1995

# Development of a Three-Dimensional Model for the Darrieus Rotor and Its Wake

R. Ganesh Rajagopalan*
*Iowa State University, Ames, Iowa 50011*
and
Dale E. Berg† and Paul C. Klimas‡
*Sandia National Laboratories, Albuquerque, New Mexico 87185*

**A computational procedure suitable for simulating the flowfield, performance, and interference of a curved-bladed, three-dimensional Darrieus wind turbine is presented. The rotor blades are modeled as time-averaged sources in the steady, laminar momentum equations solved on a Cartesian grid. As an illustration of the potential of the method, terrain and generator box influence on the behavior of the turbine are simulated in a uniform freestream wind. The generator box of the turbine is modeled as a solid cube and viscous no-slip boundary conditions are prescribed on the generator box and the ground plane. The influence of the terrain on the flowfield of the turbine is considered for two hypothetical, two-dimensional ridge-lines. Computed turbine performance, such as the power coefficient and the normal force coefficient, are compared with results from Sandia field tests and a theoretical method based on stream-tube momentum balance for a stand-alone turbine. Quantitative differences in the performance of the Sandia 17-m turbine with and without the hypothetical terrains are discussed. Qualitative behavior of the flowfield under the influence of the ground plane is also presented with the help of velocity vector plots and path lines.**

## Nomenclature

$A$ = swept area of the turbine, $0.669\ R^2$
$a$ = coefficients in the discretized momentum equations
$B$ = number of blades
$c$ = turbine blade chord
$C_l$, $C_d$ = sectional lift and drag coefficients, respectively
$C_p$ = power coefficient of the turbine, $[(\boldsymbol{T}_0 \cdot \boldsymbol{\omega})/\frac{1}{2}\rho V_\infty^3(A)]$
$d$ = discretized source term in the momentum equation
$\hat{\boldsymbol{e}}_n$, $\hat{\boldsymbol{e}}_\theta$, $\hat{\boldsymbol{e}}_s$ = unit vectors in the coordinate system $n$, $\theta$, and $s$, respectively
$\hat{\boldsymbol{e}}_r$, $\hat{\boldsymbol{e}}_\theta$, $\hat{\boldsymbol{e}}_z$ = unit vectors in the cylindrical coordinate system $r$, $\theta$, and $z$, respectively
$f$ = resultant aerodynamic force on the blade
$H$ = turbine height
$\hat{\boldsymbol{i}}, \hat{\boldsymbol{j}}, \hat{\boldsymbol{k}}$ = unit vectors in the Cartesian coordinate system $x$, $y$, and $z$, respectively
$M$ = local flow Mach number
$n$, $\theta$, $s$ = coordinate system attached to the blade
$O$ = center of turbine
$p$ = static pressure
$q_\infty$ = freestream dynamic pressure
$R$ = radius of the turbine at the equatorial plane
$Re$ = Reynolds number
$Re_c$ = Reynolds number based on blade chord and tip velocity, $(\omega R c \rho/\mu)$
$r$, $\theta$, $z$ = cylindrical coordinate system attached to the blade
$S_n$, $S_r$, $S_\theta$ = time-averaged source terms at a grid point
$S_x$, $S_y$, $S_z$ = source terms in the discretized momentum equations
$S'_x$, $S'_y$, $S'_z$ = source terms/volume in the momentum equations
$s_D$ = force due to drag per unit span along the blade
$s_L$ = force due to lift per unit span along the blade
$s_n$, $s_r$, $s_\theta$ = time-dependent source terms at a grid point
$T_0$ = torque generated at the center of the turbine
$t$ = coordinate on the time axis
$u$ = component of $V_{\text{abs}}$ in the $x$ direction
$V_{\text{abs}}$ = absolute velocity of the wind with respect to the inertial system fixed at the center of the turbine
$V_{\text{rel}}$ = relative velocity of wind observed from the reference frame fixed to the blades
$V_\infty$ = freestream wind velocity
$v$ = component of $V_{\text{abs}}$ in the $y$ direction
$v_n$ = component of $V_{\text{abs}}$ in the $n$ direction
$v'_n$ = relative normal velocity of wind observed from the reference frame fixed to the blades
$v_r$ = component of $V_{\text{abs}}$ in the $r$ direction
$v'_r$ = relative radial velocity of wind observed from the reference frame fixed to the blades
$v_\theta$ = component of $V_{\text{abs}}$ in the $\theta$ direction
$v'_\theta$ = relative tangential velocity of wind observed from the reference frame fixed to the blades
$w$ = component of $V_{\text{abs}}$ in the $z$ direction
$x$, $y$, $z$ = inertial reference frame attached to $O$, where $x$ is parallel to the freestream wind
$\alpha$ = blade angle of attack with respect to $V_{\text{rel}}$
$\dot{\alpha}$ = rate of change of angle of attack
$\delta$ = angle between the blade and the vertical
$\lambda$ = tipspeed ratio, $(\omega R/V_\infty)$
$\rho$ = density of air
$\sigma$ = solidity of the turbine, $(Bc/2R)$
$\Phi$ = general variable in the discretized momentum equation
$\omega$ = rotational velocity of the turbine

Received April 30, 1992; revision received Feb. 22, 1993; accepted for publication Jan. 6, 1994. 

*Associate Professor, Computational Fluid Dynamics Center, Department of Aerospace Engineering. Member AIAA.
†Member of Technical Staff.
‡Distinguished Member of Technical Staff.

## I. Introduction

THE Darrieus wind turbine with curved blades (see Fig. 1a for a schematic diagram) offers one of the most challenging aerodynamic problems of our times due to the complexities created by the blades rotating in crossflow. A better understanding of the aerodynamics of the Darrieus turbine would be helpful in maximizing energy capture. Also, the ability to predict the cyclic loads on the blades is crucial for fatigue calculations and cost optimization through efficient structural design. While there is a revival of interest in the alternative sources of energy in general, business interest in wind turbines is focused on wind-farms also known as wind-power parks. Designers of wind-farms require an aerodynamic analysis tool that can simulate the viscous flowfield of a farm on sites with irregular terrain and nonuniform inflow. In addition, accurate and consistent prediction of the power production potential of the wind-farm is necessary for reliable aerodynamic design, and this cannot be achieved if mutual interference of other turbines and the terrain are not considered.

Wind turbines are devices that operate within the planetary boundary layer near the ground. The ground plane retards the growth of the turbine wake affecting the inflow seen by downwind turbines. In the case of turbines with a height smaller than the planetary boundary layer the influence of the terrain on the operational characteristics of the turbine is particularly severe since the turbines are completely submerged within the shear layer of the terrain. In the last two decades aerodynamic characteristics of stand-alone, three-dimensional Darrieus wind turbines (generally, without terrain influence) have been successfully analyzed using stream-tube/momentum-based methods[1–4] and the vortex lattice method.[5] With the increase in computational power available to the scientific community and the growth of computational fluid dynamics as a viable tool for flow simulation, it appears that, at last, some of the problems associated with the flow physics of the wind turbine in realistic environments (including ground and turbine interference) can be analyzed computationally. In this vein, this investigation takes a step in the direction of actually simulating the influence of the terrain on a Darrieus rotor modeled by momentum sources.

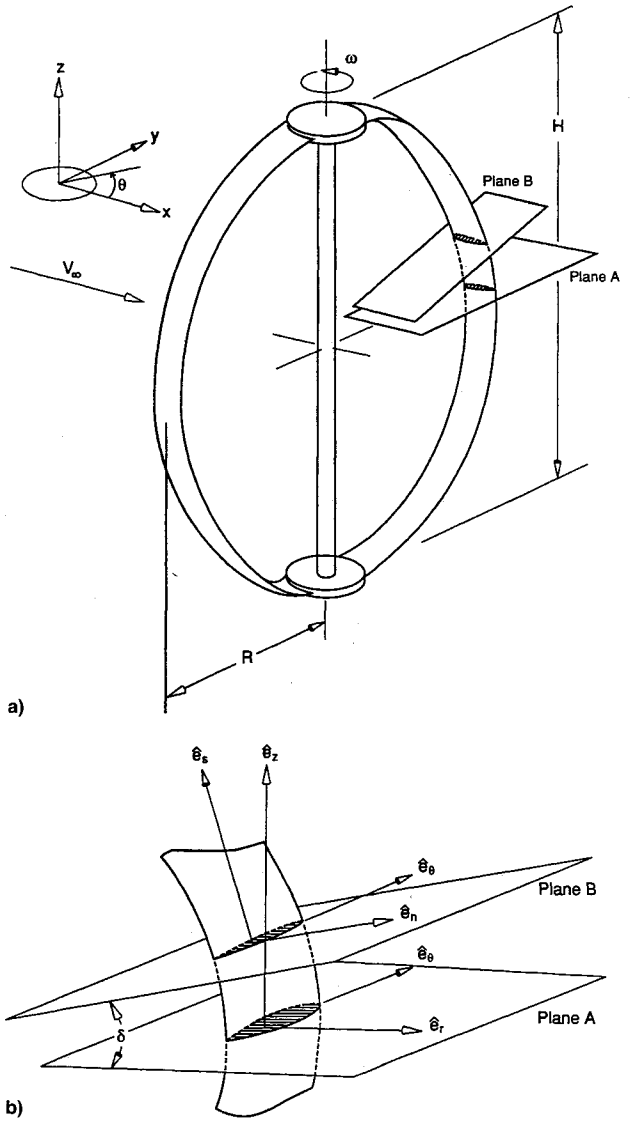


**Fig. 1 Schematic diagram of a) the rotor and coordinate system and b) the blade fixed coordinate systems.**

Rajagopalan and Fanucci[6] have demonstrated that a spinning two-dimensional vertical axis wind turbine (VAWT) can be sufficiently represented by time-averaged momentum sources in the governing flow equations. The finite difference procedure developed here, for a three-dimensional vertical axis wind turbine, is an extension and outgrowth of the above-mentioned method. This method is intermediate in complexity and accuracy between the vortex models, based on the potential flow assumption, and a possible full Navier-Stokes method with a body-fitted grid around the rotating blades embedded in a global flowfield grid. Use of the momentum sources to represent the rotating blades, admittedly, compromises the reality of the simulation very close to the blades by not resolving the (chordwise and spanwise) boundary-layer flow on the rotor. However, the ability to solve some of the currently intractable problems such as turbine-terrain interference, while avoiding the need for massive supercomputer-type numerical computations, makes this method a useful tool.

In the sections to follow the emphasis is placed on the development of the source modeling of the rotating blades of the turbine and to the coupling of these turbine sources to the Navier-Stokes (N-S) equations that govern the flow. The numerical method used solves the N-S equations, a system of coupled elliptic partial differential equations, based on a finite volume method. Solving the elliptic equations allows interference effects of interest, such as the ground plane interference, to be studied. For illustrating the potential of the method, two specific situations are considered under uniform free-stream flow: 1) a turbine with a solid generator box placed on a flat ground, and 2) a turbine and tower placed on a small two-dimensional ridge. The essentials of the method are discussed in the following sections.

## II. Numerical Algorithm

The spinning blades of the Darrieus turbine are modeled as momentum sources in the flow governing equations, and hence, a description of the equations and the numerical algorithm used in this analysis are in order.

The numerical procedure for solving the fluid flow is based on Patankar's "SIMPLER" algorithm.[7] The flowfield is determined by solving for the primitive variables $p$, $u$, $v$, and $w$ directly from the mass and momentum conservation equations (the Navier-Stokes equations). After assuming the flow to be steady, laminar, and incompressible, the Navier-Stokes equations reduce to

mass

$$\frac{\partial u}{\partial x} + \frac{\partial v}{\partial y} + \frac{\partial w}{\partial z} = 0 \tag{1}$$

$x$ momentum

$$\rho\left(u\frac{\partial u}{\partial x} + v\frac{\partial u}{\partial y} + w\frac{\partial u}{\partial z}\right) = \mu\left(\frac{\partial^2 u}{\partial x^2} + \frac{\partial^2 u}{\partial y^2} + \frac{\partial^2 u}{\partial z^2}\right) - \frac{\partial p}{\partial x} + S_x' \tag{2}$$

$y$ momentum

$$\rho\left(u\frac{\partial v}{\partial x}+v\frac{\partial v}{\partial y}+w\frac{\partial v}{\partial z}\right)=\mu\left(\frac{\partial^2 v}{\partial x^2}+\frac{\partial^2 v}{\partial y^2}+\frac{\partial^2 v}{\partial z^2}\right)-\frac{\partial p}{\partial y}+S'_y \tag{3}$$

$z$ momentum

$$\rho\left(u\frac{\partial w}{\partial x}+v\frac{\partial w}{\partial y}+w\frac{\partial w}{\partial z}\right)=\mu\left(\frac{\partial^2 w}{\partial x^2}+\frac{\partial^2 w}{\partial y^2}+\frac{\partial^2 w}{\partial z^2}\right)-\frac{\partial p}{\partial z}+S'_z \tag{4}$$

where $\mu$ is the flow viscosity and $S'_x$, $S'_y$, and $S'_z$ are the time-averaged source terms per unit volume due to the turbine's motion in the coordinate directions $x$, $y$, and $z$, respectively. $S'_x$, $S'_y$, and $S'_z$ are in addition to other source terms that may exist in the flowfield. The source terms are time-averaged for convenience and are not a requirement of the method itself as will be discussed later. These source terms denote the rotor-induced force per unit volume at a point and it is through these terms that the rotor's influence is introduced into the flowfield. Hence, we may think of the rotor being modeled as a distribution of momentum sources occurring in a specific region of the domain.

The Cartesian three-dimensional computational domain is subdivided into control volumes by a series of grid lines orthogonal to the $i$, $j$, and $k$ coordinate directions. Near the ground plane and in the vicinity of the turbine the grid points are packed to obtain better flow resolution. The flow equations, written in the conservation form, are discretized using the earlier mentioned control volume approach known by the name SIMPLER. For $\Phi$, representing any of $u$, $v$, $w$, and $p$, the discretized equation at a grid point $(i, j, k)$ is found to be

$$a_{i,j,k}\Phi_{i,j,k}=a_{i+1,j,k}\Phi_{i+1,j,k}+a_{i-1,j,k}\Phi_{i-1,j,k}+a_{i,j+1,k}\Phi_{i,j+1,k}+a_{i,j-1,k}\Phi_{i,j-1,k}+a_{i,j,k+1}\Phi_{i,j,k+1}+a_{i,j,k-1}\Phi_{i,j,k-1}+d_{i,j,k} \tag{5}$$

where $i$, $j$, $k$ are the grid indices, $a$ are the coefficients that link the neighboring $\Phi$ to $\Phi_{i,j,k}$, and $d_{i,j,k}$ is the discretized form of the source term that consists of contributions from the specific governing differential equation being discretized as well as the discretized source terms due to the action of the turbine blades. The discretized equations are solved by a line-by-line method combining the tri-diagonal matrix algorithm and the Gauss-Seidel method. In a specific number of computational cells through which the turbine blades pass, the source terms due to the turbine, $S_x$, $S_y$, and $S_z$ (discretized source terms in the respective coordinate directions $x$, $y$, and $z$, respectively), are evaluated. The development of the analytic expressions for $S_x$, $S_y$, and $S_z$ is presented next.

### A. Turbine Sources

As was mentioned earlier, the action of the turbine blades is modeled in this formulation through the momentum equation sources ($S'_x$, $S'_y$, and $S'_z$) in the coordinate directions. The rationale for this modeling procedure can be explained as follows. In addition to other things, the blades of the Darrieus turbine, as they revolve, accelerate and/or decelerate and deflect the flow. In other words, they primarily change the momentum vector of the fluid. This change in local momentum of the fluid is a direct reaction on the fluid due to the forces generated on the rotating blades. Thus, a logical place to incorporate the action of the blades in the governing equations of the fluid flow is through the source terms of the momentum equations, namely $S'_x$, $S'_y$, and $S'_z$ in the governing partial differential equations, or $S_x$, $S_y$, and $S_z$ in the discretized equations. These source terms are not known a priori and are a highly desired result of any turbine solution procedure. For example, their integration along the span of the blades, yields the performance characteristics of the turbine. Therefore, our aim here is to let the source terms develop as part of the overall solution of the entire flowfield. Since the rotating blades can be thought of as a momentum changing device, the source terms in the momentum conservation equations would accurately represent the action of the rotating blades when the flowfield is converged. In other words, when there is an overall and local conservation of momentum, the source terms would yield the proper loading on the rotor blades. The functional relation between the source terms and the local flow conditions can be developed with the help of a schematic diagram of a Darrieus turbine and a blade cross section shown in Figs. 1a and 1b, respectively.

The strength of the rotor source at a specific location through which the blade is passing is a function of the local flow conditions, the physical location, and the geometric and aerodynamic characteristics of the rotor blades. In functional notation, the time-dependent discretized source terms can be stated as follows:

$$s_x = s_x(C_l, C_d, \alpha, \dot{\alpha}, V_{\text{abs}}, \omega, x, y, z, t, c, \rho, \mu, Re, M, B) \tag{6a}$$

$$s_y = s_y(C_l, C_d, \alpha, \dot{\alpha}, V_{\text{abs}}, \omega, x, y, z, t, c, \rho, \mu, Re, M, B) \tag{6b}$$

$$s_z = s_z(C_l, C_d, \alpha, \dot{\alpha}, V_{\text{abs}}, \omega, x, y, z, t, c, \rho, \mu, Re, M, B) \tag{6c}$$

where $(x, y, z)$ denote the instantaneous blade location at time $t$. Although important, the effects of the unsteady fluctuations in angle of attack $\dot{\alpha}$ are not addressed in this preliminary investigation. It is noted here that the inclusion of the $\dot{\alpha}$ term in the formulation is possible in a limited sense through the use of a proper dynamic stall model. The influence of viscous and compressibility effects on the source terms are considered only through the airfoil aerodynamic characteristics ($C_l$ and $C_d$) used in the calculations. Therefore, the source terms can be rewritten as

$$s_x = s_x(C_l, C_d, \alpha, V_{\text{abs}}, \omega, x, y, z, t, c, \rho, B) \tag{7a}$$

$$s_y = s_y(C_l, C_d, \alpha, V_{\text{abs}}, \omega, x, y, z, t, c, \rho, B) \tag{7b}$$

$$s_z = s_z(C_l, C_d, \alpha, V_{\text{abs}}, \omega, x, y, z, t, c, \rho, B) \tag{7c}$$

For further development of the procedure we now turn to Figs. 1a and 1b. Figure 1a shows a Darrieus rotor spinning about the $z$ axis with an angular velocity $\omega$. The freestream is in the $x$ direction of the inertial coordinate system $x$-$y$-$z$ shown in the figure. The turbine's equatorial radius and height are denoted by $R$ and $H$, respectively. The planes $A$ and $B$ shown in Fig. 1a are magnified and shown with the noninertial coordinate system attached to the blades in Fig. 1b. The rotating triad $\hat{e}_r$-$\hat{e}_\theta$-$\hat{e}_z$ denotes the unit vectors corresponding to the conventional cylindrical coordinate system. The unit vectors $\hat{e}_r$ and $\hat{e}_\theta$ lie in a horizontal plane designated by plane $A$. The unit vector $\hat{e}_z$ is parallel to the axis of rotation of the Darrieus turbine. Plane $B$ is the plane that intersects the blades at a given height and radius of the rotor, and the airfoil section seen in this plane is the true section of the blades. For the convenience of force computations, another triad $\hat{e}_n$-$\hat{e}_\theta$-$\hat{e}_s$, is defined on this plane wherein $\hat{e}_n$ is normal to the airfoil section and $\hat{e}_\theta$ is in the direction tangent to the blade motion. The unit vector $\hat{e}_s$ is in the spanwise direction of the blade at the given location. If the local angle made by the blade to the vertical at the given blade section is $\delta$, then the planes $A$ and $B$ also include an angle $\delta$.

Forces due to lift and drag per unit span along the blade, in the direction of $\hat{e}_n$ at a given location, are given by

$$s_n = (s_L)_n + (s_D)_n \tag{8}$$

In terms of $V_{rel}$ seen by the blade section, $s_n$ can be further identified as

$$s_n = (c \times 1)(\rho V_{rel}^2/2)(C_l \cos \alpha + C_d \sin \alpha) \quad (9)$$

where

$$V_{rel} = (v_n'^2 + v_\theta'^2)^{1/2} \quad (10)$$

and $c$ is the blade chord and $\alpha$ is the angle of attack between $V_{rel}$ and the $\hat{e}_\theta$ vector measured positive in the conventional aerodynamic sense. Also, $v_n'$ and $v_\theta'$ are the velocity components of the relative velocity vector $V_{rel}$ measured with respect to the coordinate system fixed to the blades. The aerodynamic characteristics of the rotor blades are introduced through the complete variation of $C_l$ vs $\alpha$ and $C_d$ vs $\alpha$ for the entire range of $\alpha = 0$–$360$ deg from Ref. 8. This tabular data is interpolated for the local Reynolds number seen by the blades.

Eliminating $\alpha$ with the following relations

$$v_n' = V_{rel} \sin \alpha \quad (11)$$

$$v_\theta' = -V_{rel} \cos \alpha \quad (12)$$

one obtains

$$s_n = c(\rho V_{rel}/2)(-C_l v_\theta' + C_d v_n') \quad (13)$$

Similarly $s_\theta$, the force in the $\theta$ direction is given by

$$s_\theta = c(\rho V_{rel}/2)(C_l v_n' + C_d v_\theta') \quad (14)$$

For a time-accurate calculation these are the forces experienced by the rotor blades. However, to keep the computations to a modest level for this initial analysis, we seek only a time-averaged calculation. The time-averaging of the source terms is done as follows. The time taken by any rotor section for one revolution is given by $2\pi/\omega$, and the time taken by the blade section to go through a finite volume cell of width $\Delta\theta$ radians is $\Delta\theta/\omega$. Hence, the fractional time that any blade section undergoes the average local flow conditions at a given finite volume cell is $(\Delta\theta/\omega) \times (\omega/2\pi)$. Time-averaging $s_n$ and $s_\theta$ for $B$ blades passing through a given finite difference cell yields the time-averaged forces felt by the blades as $S_n$ and $S_\theta$ in the normal and tangential coordinate directions, respectively,

$$S_n = (c\rho V_{rel}/2)(B\Delta\theta/2\pi)(-C_l v_\theta' + C_d v_n') \quad (15)$$

$$S_\theta = (c\rho V_{rel}/2)(B\Delta\theta/2\pi)(C_l v_n' + C_d v_\theta') \quad (16)$$

where $(B\Delta\theta/2\pi)$ is the time-averaging factor that denotes the ratio of time spent by $B$ blades in traversing through a given finite volume cell to the time taken by the turbine to go through one complete revolution. In the sections to follow these are transformed to the $x$, $y$, and $z$ coordinates.

The relations between the unit vectors describing the coordinate systems fixed to the blades can be obtained from Fig. 1b as

$$\hat{e}_n = \hat{e}_r \cos \delta + \hat{e}_z \sin \delta \quad (17a)$$

$$\hat{e}_s = -\hat{e}_r \sin \delta + \hat{e}_z \cos \delta \quad (17b)$$

$$\hat{e}_r = \hat{e}_n \cos \delta - \hat{e}_s \sin \delta \quad (18a)$$

$$\hat{e}_z = \hat{e}_n \sin \delta + \hat{e}_s \cos \delta \quad (18b)$$

Since there are no aerodynamic forces in the (span) direction $\hat{e}_s$ at the blade section, the forces in the $r$ and $z$ directions become

$$S_r = S_n \cos \delta \quad (19a)$$

$$S_z = S_n \sin \delta \quad (19b)$$

Thus, the forces felt by the blades in $x$, $y$, and $z$ directions are, respectively,

$$S_x = S_r \cos \theta - S_\theta \sin \theta \quad (20a)$$

$$S_y = S_r \sin \theta + S_\theta \cos \theta \quad (20b)$$

$$S_z = S_z \quad (20c)$$

Regrouping the time-averaged source terms $S_x$, $S_y$, $S_z$ in a convenient form, suitable for use in the numerical algorithm, yields the following relations:

$$S_x = (Bc\rho/4\pi)V_{rel}\Delta\theta[C_d u - C_l(v_\theta' \cos \theta \cos \delta + v_n' \sin \theta) + C_d(v_s' \sin \delta \cos \theta + \omega r \sin \theta)] \quad (21a)$$

$$S_y = (Bc\rho/4\pi)V_{rel}\Delta\theta[C_d v - C_l(v_\theta' \sin \theta \cos \delta - v_n' \cos \theta) + C_d(v_s' \sin \delta \sin \theta - \omega r \cos \theta)] \quad (21b)$$

$$S_z = (Bc\rho/4\pi)V_{rel}\Delta\theta(C_d w - C_d v_s' \cos \delta - C_l v_\theta' \sin \delta) \quad (21c)$$

where all quantities except $B$ and $\rho$ are grid specific. These are forces per unit span acting on the blades at a finite difference cell due to the motion of the fluid passing over them. To effect an equal and opposite reaction on the fluid, these sources are subtracted from the discretized momentum equations to be solved at the finite difference cell integrated for the volume of the cell. When the iterations begin, these source terms have only a nominal value since the flow is assumed to be uniform everywhere. However, the Navier-Stokes equations are mathematically elliptic in nature, and the discretized governing equations at each cell are intimately coupled with the discretized equations at the neighboring cells. Additionally, the discretized equations for the entire domain are solved simultaneously every iteration. Thus, the disturbance to the uniform flow due to the turbine's blade motion, transmitted through the source terms of the governing equations at specific cells through which the blades pass, is felt progressively in the entire computational domain as iterations proceed. The addition of the source terms in the specific cells alters the local and global momentum balance (in all coordinate directions) initially, but as the iterations continue, the numerical value of the source terms change converging to the aforementioned momentum balance. When the solution is numerically converged, the momentum balance is complete and the flow has adjusted itself to the rotation of the turbine blades. In contrast with the stream-tube methods, this method conserves momentum in a local sense near the blades as well as in the entire computational domain in all the three coordinate directions. At best, the widely used double multiple stream-tube model conserves momentum twice within a stream-tube, once where the blades intersect the stream-tube on the upwind portion and once again where the blades intersect the stream-tube in the downwind portion. In passing, it is also important to emphasize that the turbine source terms developed in this section need be evaluated only at the specific cells through which the blades pass. The number of these specific cells is small compared to the total number of cells that describe the computational domain. This results in considerable savings in the case of multiple turbines where the computational grid requirements may remain nearly the same as the grid requirement for a single turbine. When the flow converges, the source terms, not known a priori, are also considered converged, and therefore, the force felt by the turbine blades in rotating through the fluid and all the performance characteristics of interest can be evaluated as follows.

If $f$ is the resultant aerodynamic force felt by the blades then

$$f = S_r\hat{e}_r + S_\theta\hat{e}_\theta + S_z\hat{e}_z \tag{22}$$

$$T_0 = \sum R \times f \tag{23}$$

$$C_p = [T_0 \cdot \omega/(\tfrac{1}{2}\rho V_\infty^3 A)] \tag{24}$$

where $T_0$ is the torque at the center of the turbine, $C_p$ is the power coefficient, and the summation is taken over all the cells which lie in the path of the blades.

### B. Boundary Conditions

Far upstream of the turbine, at the inlet to the computational domain, the flow is considered to be uniform. On the ground plane a no-slip boundary condition is imposed. The top boundary—a plane parallel to the ground plane with no mounds—is assumed to have freestream conditions. The downstream boundary (the far wake of the turbines and the outlet of the computational domain) values are extrapolated from the interior grid points and are adjusted to conserve mass flow through the computational domain. The generator box is modeled as a solid body with all the components of the velocity set to zero and maintained zero.

## III. Results and Discussion

Only preliminary results are presented at this time for validating the procedure. The method is robust and converges fairly quickly from an initially assumed uniform flowfield to a steady velocity field including the turbine wake. At the beginning of the iteration procedure the flow is unidirectional in the direction of the $x$ axis and velocity components in the other directions are set to zero. The converged solution yields all the three components of the velocity field and the pressure field for the entire computational domain in addition to all the turbine performance characteristics of interest. Based on a grid independence study, a (44 × 44 × 24) grid was chosen for turbine calculations with no terrain interference, and a (44 × 44 × 45) grid was deemed sufficient for turbine-terrain calculations. The computational grid actually covered a physical region of roughly (29 × 29 × 2) diameters.

A fine mesh was used in the immediate vicinity of the turbine blade path such that on the average there are about 45 grid points in the path of the blades (a full circle) at the equatorial plane. Due to the curved shape of the Darrieus rotor, the number of grid points in the neighborhood of the blades joining the axis of rotation are generally small increasing towards the equator. The inaccuracy induced as a result of a smaller number of grid points near the levels where the blades join the axis is small because the major portion of the power production is done by the blades at the equatorial plane. For all the cases considered, the number of grid points that intercepted the turbine and the overall structure of the grid in the vicinity of the swept volume of the turbine were unchanged.

The flowfield generally converged in about 250 iterations, but the performance parameters of the turbine converged as early as 50 iterations. On the NAS-9180, a (44 × 44 × 24) grid takes roughly about 35 min of Central Processor Unit (CPU) time for 250 iterations. Performance characteristics of the Sandia 17-m turbine, calculated using the procedure outlined in this article, are presented next. The geometry of the turbine was taken from Ref. 9. The density $\rho$ and viscosity $\mu$ of air were assumed to be 0.002377 slugs/ft$^3$ and 4.5638E-7 lb-s/ft$^2$, respectively.

### A. Performance Comparisons

Figures 2a–2c compare the power coefficient $C_p$ predictions from this investigation to Sandia test results[9] for turbine rotational speeds of 38.7, 46.7 and 50.6 rpm, respectively. It is

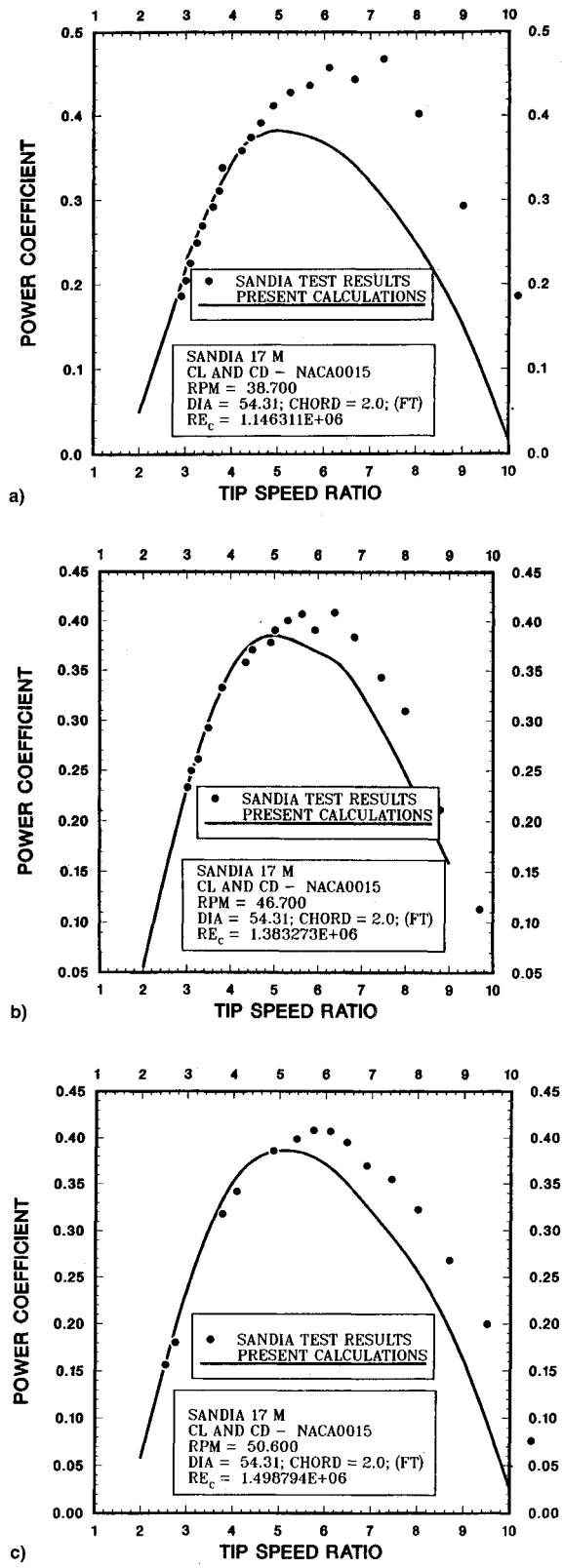


**Fig. 2 Performance comparison for rpm = a) 38.7, b) 46.7, and c) 50.6.**

observed that the agreement is only qualitative and is far from being perfect. Similar discrepancies have been observed by other researchers.[9] In the present procedure, while the flowfield is solved directly from the governing equations, the aerodynamic characteristics of the blades play an important role in the evaluation of the performance of the turbine. Hence, the agreement is largely dependent on the airfoil table[8] data used. Further analysis is necessary to determine if this data

is representative. It is suspected that the profile drag component of the airfoil table is inaccurate, since the influence of profile drag on $C_p$ is substantial. The influence of profile drag on the normal force coefficient $C_n$ is, however, minimal. This hypothesis is supported by the $C_n$ comparisons in the following discussions.

In Figs. 3a and 3b, the normal force coefficient computed at the equatorial plane is compared with the results of CARDAAV[4] (a theoretical method based on double multiple stream-tube theory), and Sandia test results[10] for tipspeed ratios $\lambda$ 3.09 and 4.60, respectively. Overall, the predictions of the present method are in better agreement with the Sandia test results than are the predictions of CARDAAV. In this diagram, $\theta = 0$ deg denotes the freestream wind direction and the segment of the curve that defines the region between $\theta = 90$ and 270 deg is the upwind region of operation of the turbine. The agreement between the theories deteriorates in the downwind regime of the turbine's operation, particularly in the range between $\theta = 270$ and 90 deg. This, in part, could be attributed to the stream-tube divergence effects not considered by the momentum-based CARDAAV as discussed below.

CARDAAV considers the cross-sectional areas of individual stream-tubes to be invariant. In other words, CARDAAV considers the sum of all the stream-tube areas intercepted by the upwind portion of the turbine to be equal to the sum of all the stream-tube areas intercepted at the downwind side. In reality, the flow through the upwind portion of the turbine slows down after a certain amount of the energy of the incoming wind has been extracted, resulting in flow divergence, through the turbine. To properly account for this divergence the area of total stream-tube interception at the upwind side must be less than that at the downwind side, and the stream-tubes should be allowed to expand in both the horizontal and vertical directions. Also, CARDAAV does not consider the induced velocity in the direction of the axis of the turbine.

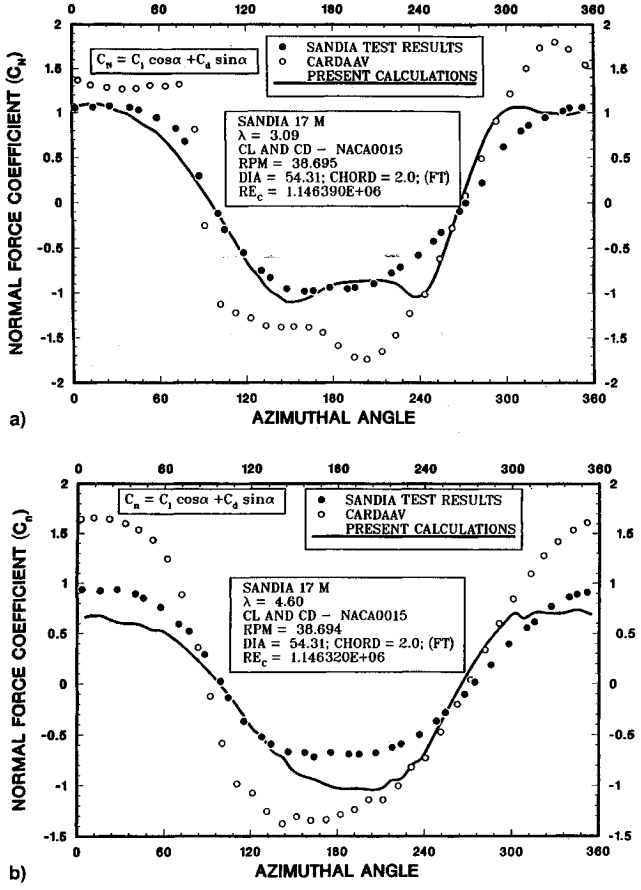


Fig. 3 Normal force comparison at the equatorial plane for $\lambda$ = a) 3.09 and b) 4.60.

### B. Interference Studies

The numerical algorithm used is an elliptic procedure and laminar viscous equations are solved to obtain the flowfield data. As a result, viscous and terrain interference effects can be studied using this procedure without any additional constraints placed on the source relations developed. To highlight the potential of the method for interference studies, the power coefficient of the turbine was calculated for a range of tip speeds $\lambda$ for the following four cases and is plotted in Fig. 4 for a constant turbine speed of 38.7 rpm.

The cases considered are 1) turbine on the flat ground without the generator box; 2) turbine and generator box on the flat ground; 3) turbine and generator box on a two-dimensional ridge (referred to as Mound1) that runs parallel to the $y$ axis of the computational domain; and 4) same as case 3 except that the mound shape was slightly altered (referred to as Mound2) while maintaining the maximum height of the ridge to be the same.

The solid generator box is modeled as a cube, 8 ft on a side. Assuming the $x$ coordinate is in the streamwise direction with the origin being at the center of the turbine, and the $y$ coordinate is normal to the plane containing the $x$ axis and the axis of rotation, the height $h$, of the two-dimensional ridge at any given $x$, $y$, is given by

$$h(x, y) = \begin{cases} 0, & \text{if } p > x \\ \dfrac{h_{\max}}{1 + \gamma(x - q)^2}, & \text{if } p \le x \le q \\ h_{\max}, & \text{if } q < x < r \\ \dfrac{h_{\max}}{1 + \gamma(x - r)^2}, & \text{if } r \le x \le s \\ 0, & \text{if } x > s \end{cases}$$

For the calculations reported here, $h_{\max} = 6$ ft, $p = -34$ ft, $q = -4$ ft, $r = 4$ ft, and $s = 34$ ft for both the ridges (Mound1 and Mound2). The shape of the ridgeline was varied by changing $\gamma$ with $\gamma = 1.0$ for Mound1 and $\gamma = 0.1$ for Mound2. The ground surface, except for a flat ground, does not mesh exactly with the Cartesian grid used. The representation for the ground surface results in a staircase-like region in the computational domain. The control volumes that lie in this region are blocked off with zero velocities everywhere. The difficulties of modeling the irregular surface using a Cartesian grid, are overcome solely by packing more grid points where

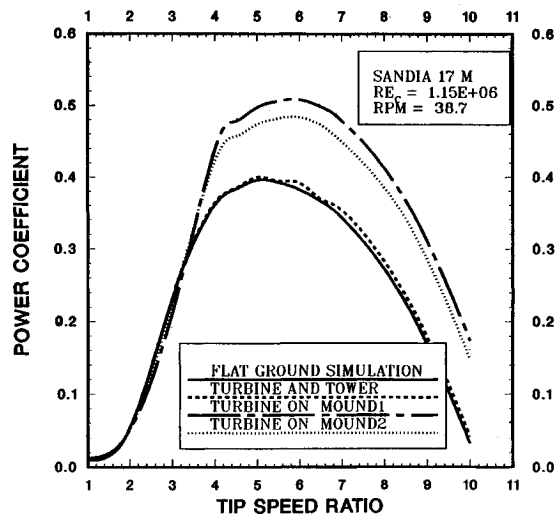


Fig. 4 Interference performance comparison.

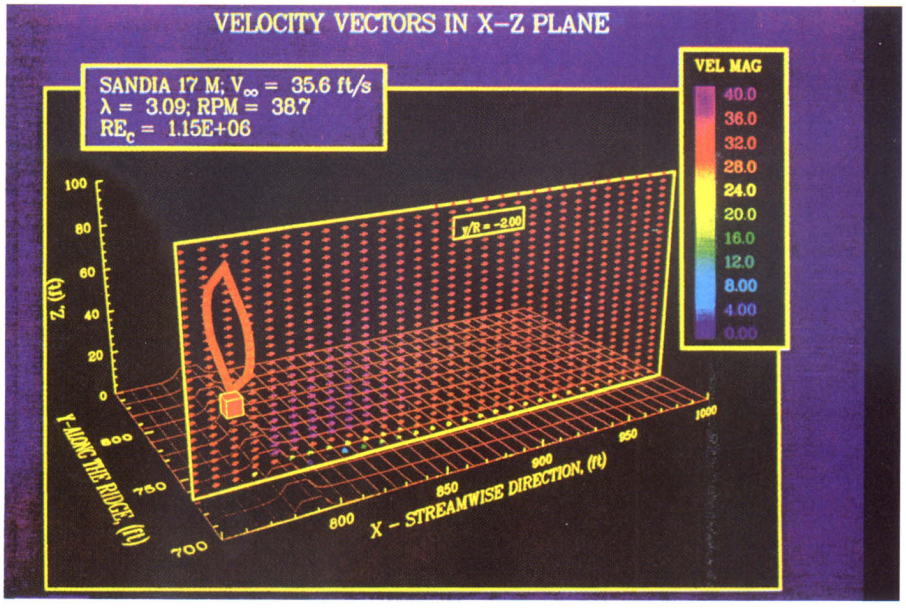


a)

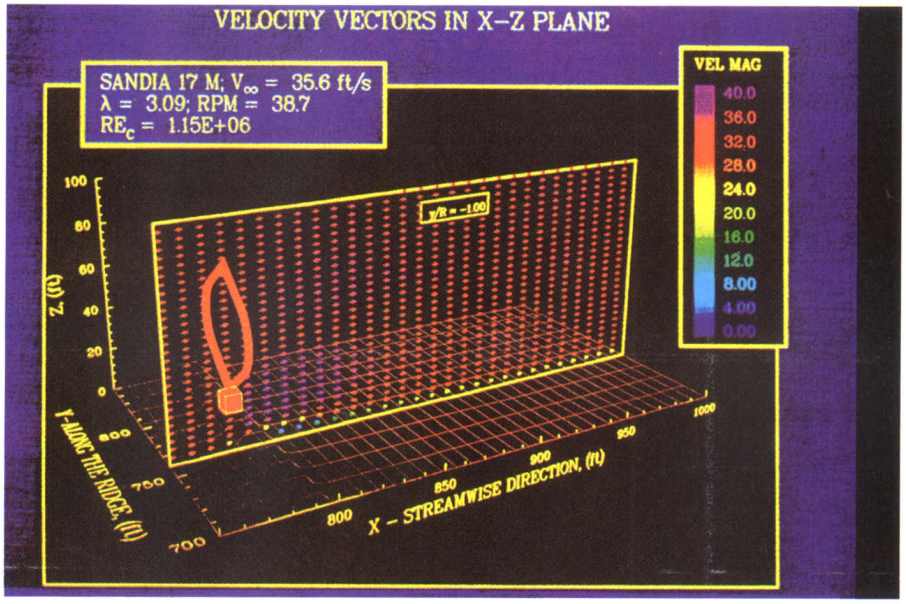


b)

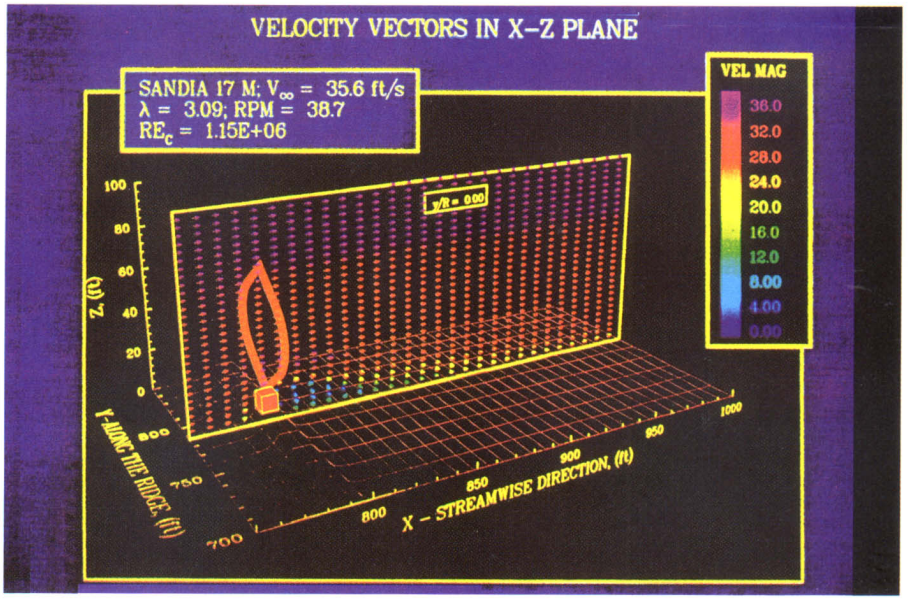


c)

**Fig. 5** Velocity vectors in the $x$-$z$ plane at $y/R$ = a) $-2.0$, b) $-1.0$, c) 0.0, d) 1.0, and e) 2.0.

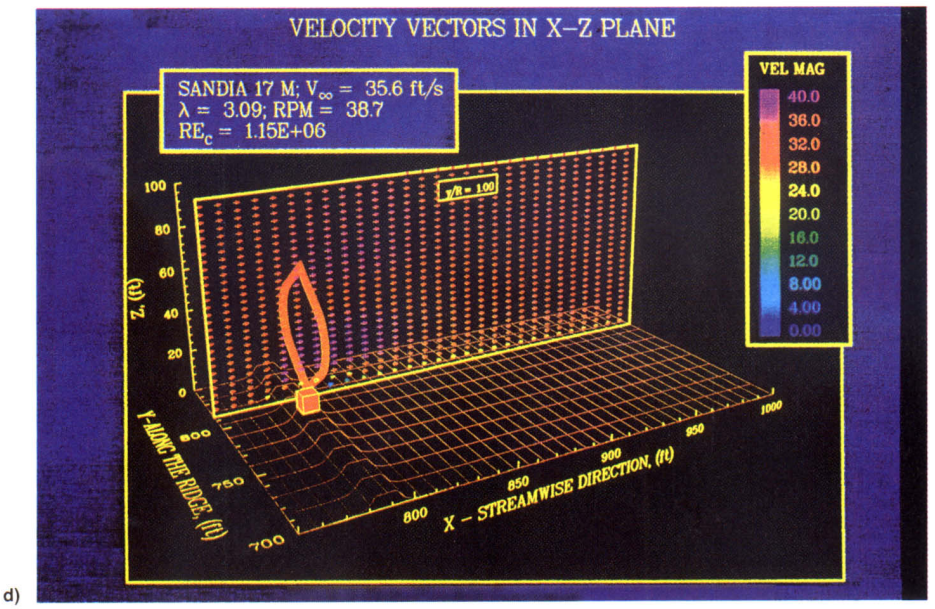


d)

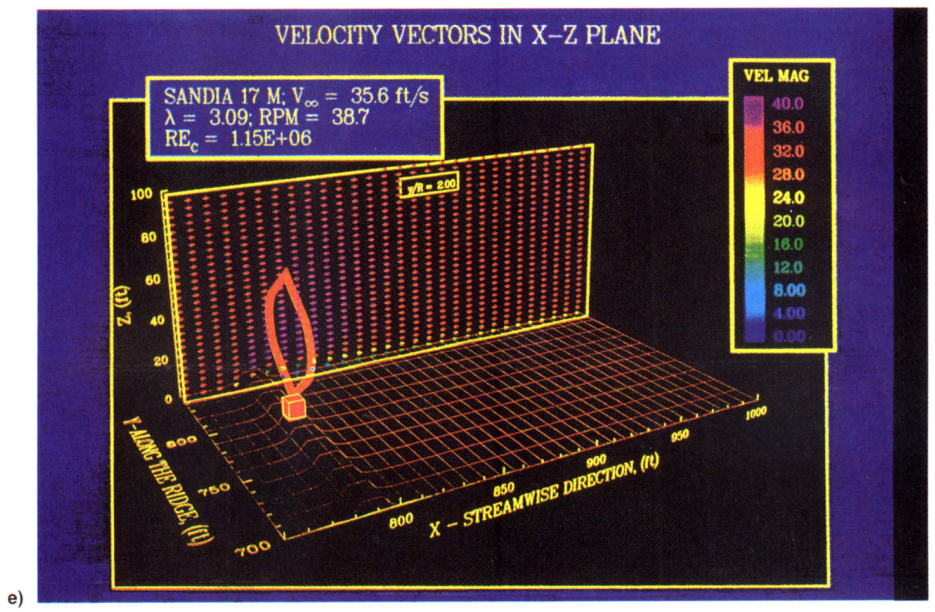


e)

**Fig. 5 (Continued) Velocity vectors in the $x$-$z$ plane at $y/R$ = a) −2.0, b) −1.0, c) 0.0, d) 1.0, and e) 2.0.**

necessary. The no-slip viscous boundary condition is enforced on all the solid surfaces, including the generator box, at all times during the computation.

No significant change in power coefficient is noticed between the turbine performances with and without the tower. At lower tip speeds, the results of all the cases reported here are nearly the same. However, as seen in Fig. 4, the power coefficient for the cases where the turbine and tower are sitting on top of the ridge are significantly higher at higher tip speeds. From this one case studied, it appears that the terrain interference and influence are more significant at higher tip speeds. A possible cause for this level of interference lies in the idealized flow situation, namely a two-dimensional ridgeline in a uniform freestream. Further analysis with various terrains and nonuniform freestream is necessary to confirm and elaborate this conclusion.

### C. Flowfield Studies

The flowfield studies reported here are for Mound1. The method developed herein provides detailed flowfield characteristics of the turbine, including the far wake. It is well known that the flow through the turbine is enclosed in a stream-tube extending from the far upstream (the capture area) to the far wake. Despite having solved for the entire Eulerian flowfield of the turbine, tracing the envelope of the above-mentioned stream-tube is no small task. In the absence of a well-established procedure to determine the boundaries of this stream-tube, the cross-plane velocity field is used to get an idea of the region of influence of the turbine. In Figs. 5a–5e the projected velocity field is depicted in cross-planes, parallel to the freestream at nondimensional distances $y/R = -2$ to $y/R = +2$. Projected direction of the velocity vectors is shown on the planes with total velocity magnitude used as a scalar to color code the vectors. The color changes indicate that the presence of the turbine is felt at distances at least 2 radii away along the $y$ axis in either direction. The upstream influence of the turbine can also be seen in Fig. 5c drawn through the axis of the turbine.

Figure 6 shows the projected direction of the vectors at the $z/H = 0$ plane (the equatorial plane). The color of the vectors indicate the velocity magnitude, and from the distribution of the colors on this plane, the spatial distribution of the velocity field at the equatorial plane can be seen to be asymmetric.

Figure 7 shows the projected direction of the vectors, color coded by the velocity magnitude, in two wake cross-planes normal to the freestream, at $x/R = 1$ (the exit plane of the

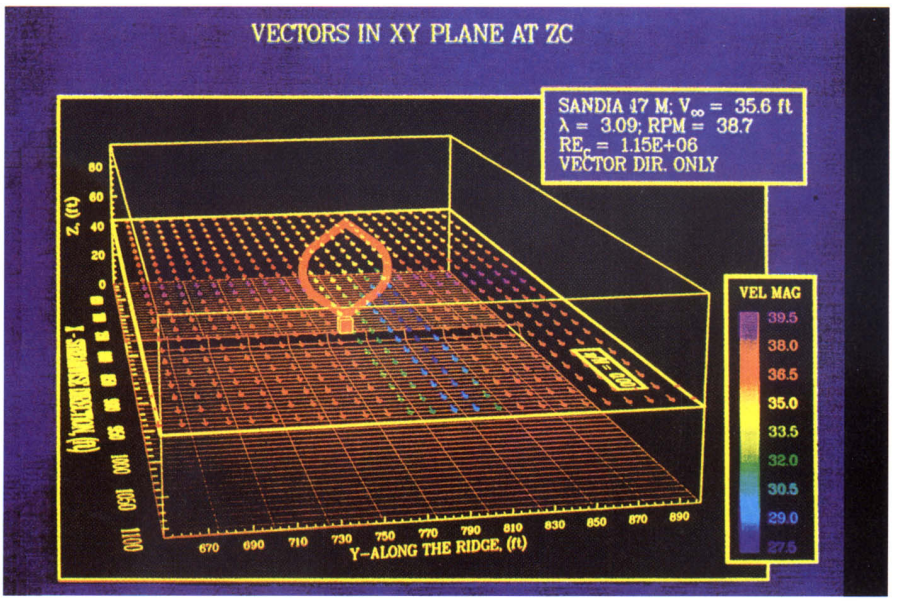


Fig. 6 Velocity vectors in the equatorial plane at $z/R = 0.0$.

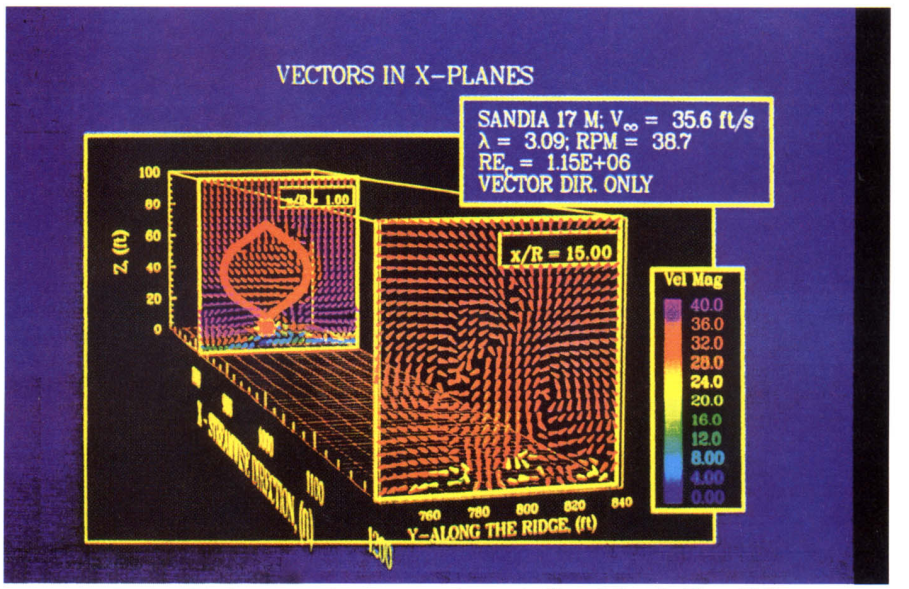


Fig. 7 Velocity vectors in two cross planes at $x/R = 1.0$ and $x/R = 15.0$.

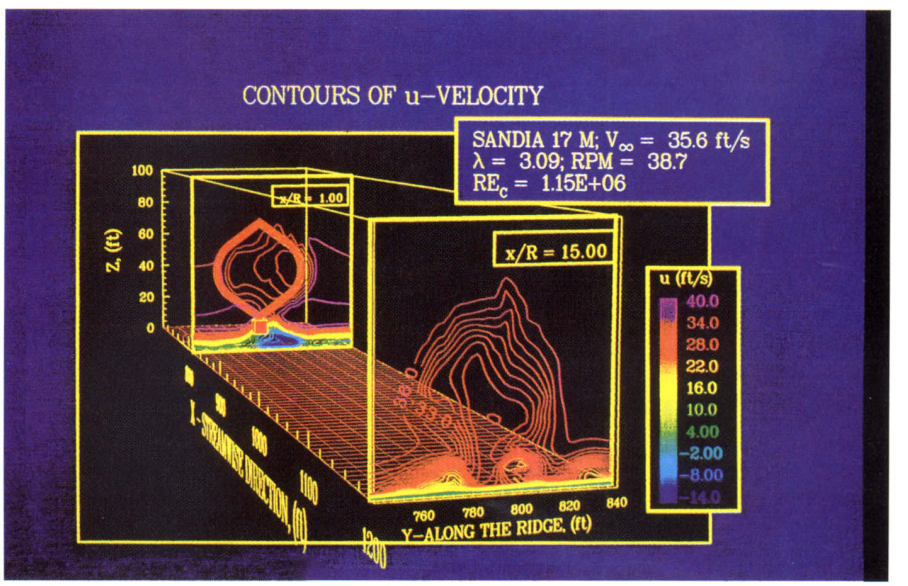


Fig. 8 Streamwise velocity contours in two cross planes at $x/R = 1.0$ and $x/R = 15.0$.

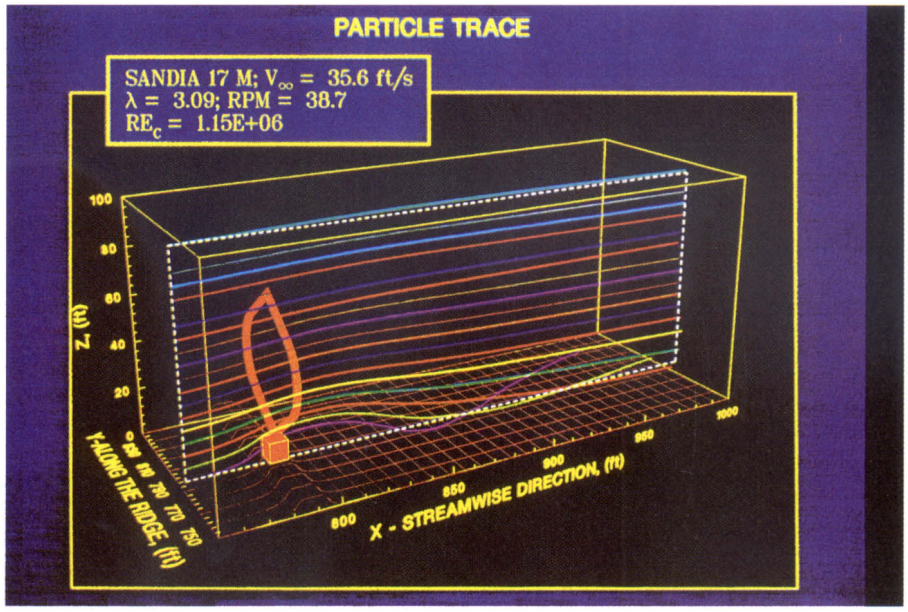


**Fig. 9 Particle traces through the rotor.**

turbine) and $x/R = 15$ (a cross-plane in the far wake). The rotational energy shed by the turbine can be seen to be mainly encapsulated in two asymmetric vortices within the streamtube discussed previously.

Figure 8 utilizes the same two planes as in Fig. 7, but displays contours of $u$ velocity (component of $V_{abs}$ in the $x$ direction—the freestream direction). The shape is highly suggestive of a self-similar profile enlarging in size as one proceeds in the direction of the wake.

### D. Particle Traces

Until now our interest in the flowfield was dominated by the velocity field of the flow through the turbine. To gain further insight into the behavior of the flow through the turbine we look at material lines or particle traces. For a steady flow, these particle traces also represent streamlines. The particle traces presented here in Fig. 9 are computed using a second-order algorithm briefly described in the Appendix. The particles are released directly upstream of the turbine in a vertical line parallel to the $z$ axis and lying in the plane parallel to the freestream passing through the axis of the turbine. The rectangle formed by the white dotted line represents the plane that would be formed by these particles if they were not disturbed by the turbine. The path lines close to the ground show the influence of the ridge and the generator box by curving around them. The same path lines can also be seen to oscillate about the plane ($y/R = 0$) in the wake, suggesting the oscillatory nature of the flow itself in the proximity of the ground.

## Conclusions

A finite difference source modeling procedure has been developed for simulating the flowfield, performance, and interference of the curved-bladed Darrieus turbine. As an illustrative study, the laminar flowfield of the Sandia 17-m turbine has been generated with a generator box and hypothetical ridge-lines. The two-dimensional ridge-line is shown to have a significant influence on the performance of the turbine at higher tip-speed ratios. The magnitude of this influence is to be interpreted in the light of the idealizations used in this study, namely a two-dimensional ridge-line and a uniform freestream wind with no ground shear. Further improvements can be made by including a digitized description of the topography, with a body-fitted grid layout, to accurately simulate the flowfield of the vertical axis wind turbine. This research, although a significant improvement in simulating the flowfield of a wind turbine, will be complete only if ground shear in the incoming velocity profile and turbulence modeling are introduced in the modeling.

## Appendix: Particle Tracing Algorithm

Once the steady Navier-Stokes equations have been solved, by definition we know the Eulerian velocity vector field in the form

$$V = [u(x, y, z), v(x, y, z), w(x, y, z)]$$

A simple first-order procedure to obtain the trace of a particle at a given point $\boldsymbol{r} = (x, y, z)$ would be to assume that the Eulerian velocity at that point is the constant velocity of the particle sweeping through $\boldsymbol{r}$ during an infinitesimal passage of time $\Delta t$. Then integrating

$$\frac{d\boldsymbol{r}}{dt} = V$$

we get the change in position of the fluid particle as

$$\Delta \boldsymbol{r} = V\Delta t$$

This procedure can be repeated with the known velocity components at the new location and in this manner the path-line followed by the particle can be obtained. While this procedure may be satisfactory for flows where the velocity gradients are small, a turbine's primary role is to change the momentum of the fluid particle significantly. Hence, a higher-order formulation is desirable for accommodating the large spatial changes in velocity, particularly in the vicinity of the turbine. Rather than assuming the velocity $V$ to be constant during the interval $\Delta t$, we assume that the acceleration of the particle $\boldsymbol{a}$ is a constant. The acceleration of a particle at a given instant is again assumed to be the Eulerian acceleration at the point in the field which the particle occupies at that instant, and this can be obtained by taking the material derivative of the velocity as follows:

$$\boldsymbol{a} = \frac{DV}{Dt} = \frac{\partial V}{\partial t} + V \cdot \nabla V$$

Assuming this acceleration to be constant over an interval $\Delta t$,

we can obtain, using elementary particle mechanics, the change in the particle's position as

$$\Delta r = V\Delta t + a[(\Delta t)^2/2]$$

Repeating this process at the new location and continuing further in the same manner, the path of a particle can be traced starting from any given location.

## Acknowledgments

Financial support for the project was provided in part by Sandia National Laboratories and the Engineering Research Institute of Iowa State University. The authors wish to acknowledge the local computing that was provided by the Iowa State Computation Center as part of a block grant and the supercomputer time that was provided by NASA through a grant under the National Aerodynamic Simulation Program. The authors are grateful to the reviewers for their many invaluable suggestions for revising the manuscript. This article is dedicated to J. B. Fanucci.

## References

[1]Templin, R. J., "Aerodynamic Theory for the NRC Vertical Axis Wind Turbine," National Research Council, LTR-LA-160, Canada, June 1974.

[2]Strickland, J. H., "The Darrieus Turbine: A Performance Prediction Model Using Multiple Streamtubes," Sandia Lab. Rept., SAND 75-0431, Albuquerque, NM, Oct. 1975.

[3]Shankar, P. N., "On the Aerodynamic Performance of a Class of Vertical Shaft Windmills," *Proceedings of the Royal Society of London, Section A*, 349, 1976, pp. 35–51.

[4]Paraschivoiu, I., and Delclaux, F., "Double Multiple Streamtube Model with Recent Improvements," *Journal of Energy*, Vol. 7, May–June 1983, pp. 250–255.

[5]Strickland, J. H., Smith, T., and Sun, K., "A Vortex Model of the Darrieus Turbine: An Analytical and Experimental Study," Sandia Lab. Rept., SAND 81-7017, Albuquerque, NM, June 1981.

[6]Rajagopalan, R. G., and Fanucci, J. B., "Finite Difference Model for Vertical Axis Wind Turbines," *Journal of Propulsion and Power*, Vol. 1, No. 6, 1985, pp. 432–436.

[7]Patankar, S. V., "Numerical Heat Transfer and Fluid Flow," Hemisphere, McGraw–Hill, Washington, DC, 1980.

[8]Sheldahl, R. E., and Klimas, P. C., "Aerodynamic Characteristics of Seven Symmetrical Airfoils Sections Through 180-Degree Angle of Attack for Use in Aerodynamic Analysis of Vertical Axis Wind Turbine," Sandia Lab. Rept., SAND 80-2114, Albuquerque, NM, March 1981.

[9]Wilson, R. E., and Walker, S. N., "Fixed Wake Analysis of the Darrieus Rotor," Sandia Lab. Rept., SAND 81-7026, Albuquerque, NM, Nov. 1980.

[10]Worstell, M. H., "Aerodynamic Performance of the DOE/Sandia 17-m Vertical Axis Wind Turbine in the Two-Bladed Configuration," *Journal of Energy*, Vol. 5, Jan.–Feb. 1981, pp. 39–42.